Journal of Molecular Liquids 366 (2022) 120267

Contents lists available at ScienceDirect

Journal of Molecular Liquids

journal homepage: www.elsevier.com/locate/molliq

Oxytetracycline removal and *E. Coli* inactivation by decomposition of hydrogen peroxide in a continuous fixed bed reactor using heterogeneous catalyst

Tetiana Tatarchuk [a,b,*], Nazarii Danyliuk [a], Ivanna Lapchuk [a], Wojciech Macyk [b], Alexander Shyichuk [a,c], Roman Kutsyk [d], Volodymyr Kotsyubynsky [e], Volodymyra Boichuk [e]

[a] Educational and Scientific Center of Material Science and Nanotechnology, Vasyl Stefanyk Precarpathian National University, Ivano-Frankivsk 76018, Ukraine
[b] Faculty of Chemistry, Jagiellonian University, ul. Gronostajowa, 2, 30-387 Kraków, Poland
[c] Faculty of Chemical Technology and Engineering, Bydgoszcz University of Science and Technology, Bydgoszcz, Poland
[d] Microbiology Department, Ivano-Frankivsk National Medical University, Ivano-Frankivsk 76018, Ukraine
[e] Department of Material Science and New Technology, Vasyl Stefanyk Precarpathian National University, 76018 Ivano-Frankivsk, Ukraine

ARTICLE INFO

Article history:
Received 6 August 2022
Revised 25 August 2022
Accepted 31 August 2022
Available online 5 September 2022

Keywords:
Fenton oxidation
Hematite
Hydrogen peroxide
Fixed-bed reactor
Water disinfection
Oxytetracycline

ABSTRACT

Fenton oxidation with heterogeneous hematite catalyst in a fixed bed reactor was investigated for water disinfection. The granulated hematite catalyst was prepared and tested to decompose H_2O_2, inactivate bacteria *E. coli* and degrade oxytetracycline. X-ray diffraction patterns confirmed the stability of the catalyst phase after sintering and after the decomposition of H_2O_2. Mössbauer spectra of the raw and used catalysts demonstrate the stable values of isomer shift. This fact confirms the chemical stability of the hematite catalyst. The degree of the H_2O_2 decomposition was found to increase with increasing residence time in the catalytic reactor. The prepared hematite catalyst was tested for the removal of oxytetracycline in a continuous flow mode. The efficiency of oxytetracycline removal increases with the increasing concentration of H_2O_2. The effect of the inlet concentration of H_2O_2 on the inactivation of *E. coli* was also studied. It was found that the outlet bacterial count gradually decreases with the increase of the inlet H_2O_2 concentration. The larger the inlet bacterial loading, the larger the H_2O_2 concentration is required to attain an acceptable bacteria count at the reactor outlet. At neutral pH, the surface of the catalyst is positively charged (pH_{PZC} = 8.09) and *E.coli* bacteria are electrostatically attracted to the hematite surface. This contributes to their accelerated inactivation by hydroxyl radicals formed on the catalyst surface. Thus, the fixed-bed flow-through reactor filled with hematite is promising for the degradation of organic pollutants and water disinfection.

1. Introduction

Water purification and disinfection are one of the key challenges of humanity. About 1.8 billion people use contaminated water that is unfit for human consumption [1,2]. The main sources of bacterial and organic pollution are municipal, hospital, and industrial wastewaters. The number of cases of bacterial infections reaches two million per year. The pathogenicity of bacteria largely depends on the structure of their outer shell cellular wall [3]. So-called Gram-positive bacteria have a straight thick cell wall, while Gram-negative bacteria have a multilayer cell wall [4]. It is the Gram-negative bacteria that often cause infectious diseases. *Escherichia coli* is a common Gram-negative bacterium found in the aquatic environment. *E. coli* usually occurs in the digestive tract of animals and humans and is not harmful to healthy organisms. However, even non-pathogenic strains of *E. coli* may cause an infectious disease with a weak immune system [5]. The most common water disinfectants are chlorine gas and ozone, but both have disadvantages. Molecular chlorine reacts with organic matter to form toxic by-products. Ozone, on the other hand, requires complex equipment, is unstable, and is expensive. For this reason, hydrogen peroxide is considered a promising reagent for disinfecting water.

Hydrogen peroxide is a usual oxidizing agent in advanced oxidation processes (e.g., Fenton processes) for the treatment of industrial wastewaters [6–11]. The well-known Fenton oxidation is highly efficient and easy to use [12]. However, homogeneous Fenton oxidation has disadvantages related to the required acidic

* Corresponding author.
E-mail address: tetyana.tatarchuk@pnu.edu.ua (T. Tatarchuk).

https://doi.org/10.1016/j.molliq.2022.120267
0167-7322/

pH and the formation of iron hydroxide by-products. Instead, heterogeneous Fenton oxidation with iron-containing solid catalysts looks better due to the easy separation and reuse of the catalyst [13,14]. As in the case of the homogeneous Fenton catalyst, the interaction of hydrogen peroxide with iron ions at the catalyst surface leads to the formation of hydroxyl radicals capable of destroying various organic pollutants and microorganisms [14,15]. The heterogeneous Fenton catalysts do not require low pH conditions, reducing operating costs and environmental issues [12]. During heterogeneous Fenton oxidation, only small amounts of iron ions are leached from the catalyst surface [16].

Among iron oxides, hematite Fe_2O_3 attracts attention due to its abundance, low cost, and stable catalytic activity [17–19]. The catalytic performance of the hematite catalysts depends mainly on several factors, such as concentration of surface active centers, the size of the available pores, the chemical and thermal stability of the structure [20,21]. The mechanism of H_2O_2 catalytic decomposition on the hematite surface is still under study [22–26]. The main reaction of the catalytic cycle is the generation of hydroxyl radicals by oxidation of ferrous ions present on the hematite surface:

$$\equiv Fe^{2+} + H_2O_2 \rightarrow \equiv Fe^{3+} + HO^{\bullet} + HO^{-} \quad (1)$$

Ferrous ions are formed *via* the reduction of ferric ions by H_2O_2:

$$\equiv Fe^{3+} + H_2O_2 \rightarrow \equiv Fe^{2+} + HOO^{\bullet} + H^{+} \quad (2)$$

The reaction (2) is much slower and therefore limits the overall reaction rate [23]. The formed hydroxyl radicals $HO^{\bullet}$ are highly reactive species that effectively destroy organic molecules while hydroperoxyl radicals $HOO^{\bullet}$ are less effective oxidants. Hydroxyl radicals can also react directly with hydrogen peroxide:

$$HO^{\bullet} + H_2O_2 \rightarrow HOO^{\bullet} + H_2O \quad (3)$$

It is worth noting that literature reports use the Fenton oxidation mainly in batch mode. However, batch reactors have some disadvantages, like difficulties in separating the catalyst from the aqueous medium [27]. On the other hand, the flow-through reactors with heterogeneous Fenton catalysts can effectively decompose organic pollutants and inactivate pathogenic microorganisms [28–31]. Punathil et al. [32] used an iron catalyst supported with activated carbon in a fixed bed reactor to degrade methylene blue. Munoz et al. [33] used magnetite Fe_3O_4 as a catalyst to remove cylindrospermopsin cyanotoxin from pharmaceutical wastewater. Xu et al. [34] studied the magnetic composite catalyst containing sepiolite and Fe_3O_4 as a fixed-bed catalyst to degrade bisphenol A. Vu et al. [35] studied mesoporous composite $Fe_2O_3{\cdot}SiO_2$ as a fixed-bed catalyst to remove tartrazine. Zolfaghari et al. [36] studied the continuous flow reactor filled with the heterogeneous bio-Fenton catalyst Fe_3O_4/TiO_2 on the graphite oxide surface to remove the malachite green dye. Literature reports do not indicate the significant leaching of iron ions from the catalyst surface. However, the long use of a batch reactor for the oxidation of organic pollutants can lead to the accumulation of organic acids, poisoning of the catalyst, and its corrosion.

The hematite has been reported to have innate antibacterial properties [16,37–41]. Several studies confirm the antibacterial effect of hematite in disinfection processes [42,43]. Fe_2O_3 has been reported to be effective against Gram-positive bacteria [44]. Numerous studies are aimed to use hematite for disinfecting water. For example, Bhushan et al. [45] synthesized an α-Fe_2O_3/Co_3O_4 nanocomposite and described its antimicrobial properties against *E. coli, B. subtilis, S. aureus,* and *S. Typhi.* The bactericidal activity of the obtained material was explained by the synergistic action of both oxides. Rufus et al. [42] synthesized an antibacterial hematite sample using a "green" method with the use of *Anacardium occidentale* extract. *Escherichia coli* and *Staphylococcus aureus* were inactivated successfully. The biocide test was performed using the agar-well diffusion method. A similar method was used to assess the antibacterial properties of α-Fe_2O_3 oxide [43]. Inhibition zones of 16 and 14 mm were observed for *S. aureus* and *E. coli*, respectively.

Oxytetracycline is an industrial antibiotic used to combat a wide range of pathogenic microbes in intensive livestock, poultry and fish farming [46]. OTC is harmful when released into the environment as it favors the proliferation of antibiotic-resistant genes [47,48]. OTC molecule contains four rings with a number of functional groups [49]. The conventional wastewater treatment methods cannot effectively remove OTC due to its intrinsic resistance to bacterial degradation. For this reason, a lot of research is aimed at developing efficient and environmentally friendly technologies for OTC removal at source. The most studied methods are adsorption, ozonation and photocatalytic oxidation [50,51]. Advanced oxidation with hydrogen peroxide or persulfate also shows promise due to the use of inexpensive oxidants and a minimal amount of by-products formed [52,53]. Iron-containing compounds have been found to effectively catalyze oxidation of OTC by hydrogen peroxide [54,55]. The oxidizing action of hydrogen peroxide is maximal in the optimal concentration range, above which the side reaction of hydrogen peroxide with hydroxyl radicals intensifies [50]. The main pathways of OTC oxidation are hydroxylation, oxidation of alcohol and phenolic hydroxyl groups, demethylation, decarbonylation and dehydration [50,56]. It is worth noting that most of the research was conducted in batch mode, which is not convenient for large-scale applications.

The aim of this work is to evaluate a fixed-bed flow reactor filled with hematite as a heterogeneous Fenton catalyst. Model water pollutants were the antibiotic oxytetracycline and *Escherichia coli* bacteria. The effect of hydrogen peroxide concentration on the removal of oxytetracycline and the inactivation of *Escherichia coli* was assessed.

2. Materials and methods

2.1. Chemicals and microorganisms

Reagent grade iron oxide Fe_2O_3 and hydrogen peroxide (31.5 %) were obtained from SferaSim (Ukraine). Oxytetracycline (OTC) was obtained from Klebrig Co. ltd. (China). The model bacteria were Gram-negative, non-spore-forming bacteria *Escherichia coli (ATCC 35218).*

2.2. Catalyst preparation and characterization

The hematite powder was pressed into pellets of 1 cm in diameter (at pressure 2 kN) and sintered at 900 °C for 6 h. The sintered pellets were crushed and sieved to obtain granules of irregular forms with sizes from 0.2 to 2 mm. The obtained Fe_2O_3 granules were stable in hydrogen peroxide solutions and did not show spontaneous leaching of iron ions. The following labeling was used throughout the study: the as-obtained sample was labeled as "raw-Fe_2O_3"; the sintered granulated sample was labeled as "sintered-Fe_2O_3", and the catalyst granules recovered after the catalytic reaction was labeled as "used-Fe_2O_3".

The phase compositions of the catalyst samples were determined using a Shimadzu XRD-7000 diffractometer ($\theta - 2\theta$ scheme) equipped with a Cu-K_α radiation tube (λ = 1.5418 Å) operating at 35 kV and 40 mA. The full pattern Rietveld refinement was performed using FullProf software.

The mean size of the Fe_2O_3 particles has been estimated from the Scherrer equation: $D = 0.89\lambda/\beta\cos\theta$, where λ is the X-ray

wavelength; β is the line broadening in radians, and θ is the Bragg angle. β was calculated according to the Gaussian profile: $\beta^2 = \beta^2_{exp} - \beta^2_{inst}$, where β_{exp} is line broadening at half the maximum intensity (FWHM) and β_{inst} is the instrumental broadening (determined from the lanthanum hexaboride LaB_6 standard). The FWHM of the 210-$K_{\alpha 1}$ reflex for the LaB_6 standard defines β_{inst} for the diffraction system and was equal to 0.046°.

^{57}Fe Mössbauer spectra were obtained using the MS1104Em spectrometer with the constant acceleration and moving absorber (^{57}Co source with an activity of about 10 mCi). Spectra were recorded at room temperature in the transmission geometry. ^{57}Fe thin absorber demonstrates a linewidth of 0.29 mm/s. The isomer shift was calibrated according to α-Fe at room temperature. The velocity resolution was about 0.008 mm/s per channel. The resulting signal-to-noise ratios were greater than 31. The hyperfine parameters were obtained from the Mössbauer spectra using UnivemMS 7.01 software. The spectra analysis was made under the assumption of the same width of all spectrum lines.

The morphology and elemental composition of the samples were examined using a REMMA-102–02 scanning electron microscope equipped with a tungsten cathode with an accessory for energy dispersion analysis. The accelerating voltage was approximately 20 kV.

The point of zero charge (pH_{PZC}) of hematite granules was measured by the pH drift method. Solutions of sodium chloride (0.1 M) with different pH values were prepared. The pH value was adjusted by adding a solution of hydrochloric acid (pH < 7) and sodium hydroxide (pH greater than 7). Then 0.3 g of hematite sample was added to 10 mL of each solution. The solutions were stirred for 4 h at room temperature and left for 24 h. The final pH values were plotted as pH_{final} *vs* $pH_{initial}$. The pH_{PZC} value of the catalyst surface was determined as the point of intersection of the experimental curve with the line $pH_{initial} = pH_{final}$.

2.3. Testing the catalytic activity of hematite in batch and flow modes

In the batch mode, the catalytic decomposition of hydrogen peroxide was tested at 20 °C using a 100 mL beaker under continuous stirring at 1000 rpm. The initial H_2O_2 concentration was 100 mM. The dosage of the Fe_2O_3 catalyst was 2 g/L. The reaction mixture was sampled using a syringe filter and residual concentrations of H_2O_2 were measured at 240 nm using a ULAB 102-UV spectrophotometer. Continuous measurements of the oxidation–reduction potential (ORP) were carried out using a combined platinum/silver chloride electrode with a PH800 laboratory benchtop pH meter (Apera Instruments).

The continuous flow tests were performed in the tubular reactors filled with the sintered-Fe_2O_3 catalyst granules. The flow-through reactors were polymeric tubes capped with mineral wool filters and stoppers. Three reactors were tested having different lengths and internal diameters (Table 1). The different internal volumes of the reactors resulted in different times of contact with the catalyst. The residence time (RT) was calculated by the following formula [57]: $RT = \frac{V_r - V_c}{j}$, where V_r is the volume of the fixed-bed reactor (mL), V_c is the volume of the hematite catalyst (mL), j is the flow rate (mL/min).

Table 1
Reactor dimensions and details of catalytic experiments.

parameter	reactor A	reactor B	reactor C
internal diameter of the tube, mm	3.5	12	12
column length, mm	200	290	650
empty reactor volume, mL	1.9	32.8	73.5
mass of catalyst (Fe_2O_3), g	0.5	57	144
size of catalyst particles, mm	0.2 … 2.0	0.2 … 2.0	0.2 … 2.0
bulk catalyst density, g/cm^3	5.1	5.1	5.1
fluid flow rate, mL/min	4.5	4.5	4.5
residence time (RT), min	0.5	4.7	10.5
H_2O_2 concentration, mM	2 … 5	2 … 5	2 … 5

2.4. Oxytetracycline degradation tests

Hydrogen peroxide solution and oxytetracycline solution were simultaneously fed to the reactor by peristaltic pumps with the total flow rate of 4.5 mL/min. The experimental runs were carried out at room temperature (20 °C). The oxidative degradation of oxytetracycline was studied using different inlet concentrations of hydrogen peroxide (10–20 mM) and OTC (2–6 mg/L). The outlet concentration of OTC was determined by spectrophotometry using ULAB 102-UV spectrophotometer with quartz cuvettes of 20 mm optical path. UV spectrum of OTC contains two peaks appropriate for its quantitative determination (Fig. 1a). The peak at 278 nm overlaps the spectrum of H_2O_2 which is also present in the solution (Fig. 1b). However, the OTC peak at 356 nm is free from this interference. Samples of the reaction mixture were analyzed in triplicate and the results were averaged.

|The effects of OTC and H_2O_2 concentrations on degradation efficiency were described by the response surface method (RSM). The modeling was carried out using the software Design-Expert (ver. 8.0.6). The used levels of the independent variables form a 3 × 5 matrix (Table 2).

2.5. Bacterial inactivation tests

Bacteria *Escherichia coli* were plated on an agar medium under sterile conditions and grown at 37 °C for 24 h. The grown colonies were used to prepare a bacterial suspension, which was normalized according to the turbidity standard. Serial dilutions of the bacterial suspension were made by adding 0.1 mL of the bacterial suspension to 0.9 mL of saline. The resulting solution was added to 1 L of distilled water to obtain the desired concentration ranging from 10^3 to 10^5 CFU/L. The concentrations of hydrogen peroxide solution, used for bacterial inactivation, were 10, 25, 50, 100, 150, and 200 mM. Hydrogen peroxide solution and bacterial dispersion were simultaneously fed to the reactor by peristaltic pumps with the total flow rate of 4.5 mL/min. All experiments have been performed at room temperature (20 °C). Bacteria remaining in the reactor effluent were collected using a membrane filter. The filter was placed on Endo medium and kept at 37 °C for 24 h. The Endo medium contains lactose which is fermented by *Escherichia coli*. The formed red colonies with a characteristic metallic sheen have been counted. The control bacterial suspension was the one that did not flow through the reactor. Log inactivation was calculated using the equation (4):

$$Log\ inactivation = log(N_{in}/N_{out}), \quad (4)$$

where N_{in} and N_{out} are the bacterial concentrations (CFU/L) at the inlet and the outlet of the catalytic reactor, respectively. The inactivation percentage (%) was calculated using the equation (5):

$$\%\ inactivation = [1 - N_{out}/N_{in}] \times 100\% \quad (5)$$

3. Results and discussion

3.1. Characterization of the catalyst

3.1.1. XRD

X-ray diffractometry was used to assess the phase composition and stability of the catalyst samples. Fig. 2a shows the XRD patterns of the raw-Fe_2O_3, sintered-Fe_2O_3, and used-Fe_2O_3. All Bragg

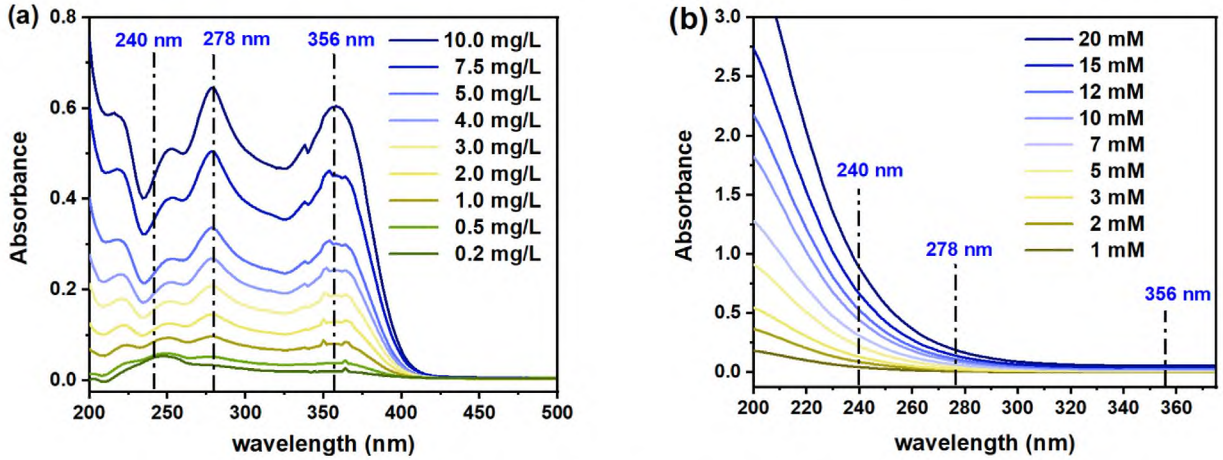

Fig. 1. (a) UV–vis spectra of OTC solutions with indicated concentrations; (b) UV spectra of H_2O_2 solutions with indicated concentrations.

Table 2
The levels of the independent variables used in the RSM modeling.

independent variable	levels
[OTC], mg/L	2; 3; 4; 5; 6
[H_2O_2], mM	10; 15; 20

peaks of the XRD patterns correspond to the only rhombohedral structure of α-Fe_2O_3 (PDF# 87–1164). The presented data show that the hematite phase remained stable after sintering and after the catalytic decomposition of H_2O_2.

The full width at half maximum (FWHM) of diffraction peaks was found to decrease after sintering (Fig. 2b). However, FWHM again increased after the use of hematite catalyst in the decomposition of H_2O_2 (Fig. 2b). The changes in FWHM mean that the average crystallite size is changed. The average crystallite sizes of the raw-Fe_2O_3, sintered-Fe_2O_3, and used-Fe_2O_3 samples were calculated according to the Scherrer equation. The crystallite size values were found to be 41, 47, and 35 nm, respectively. The increase in crystallite size after sintering can be explained by considering that the raw hematite sample contains surface OH groups formed from adsorbed water molecules. During sintering, the surface OH groups are lost and crystallite boundaries become more ordered. The opposite changes occur during the catalytic decomposition of H_2O_2. The formed hydroxyl radicals lead to the hydroxylation of the hematite surface. As a result of the partial amorphization, the average crystallite size of the used-Fe_2O_3 is decreased. The sintering treatment does not change the lattice parameters *a* and *c* (the *a* value is equal to 5.03 Å, while the *c* value is equal to 13.74 Å). The lattice parameters *a* and *c* did not change after the catalytic decomposition of H_2O_2.

3.1.2. Mössbauer spectroscopy

Fig. 3 shows the room-temperature Mössbauer spectra of the hematite samples obtained in transmission mode. All the spectra were optimally adjusted by using only one sextet component. Table 3 summarizes the results of the spectra fitting. The slightly decreased quadruple splitting after sintering corresponds to increased crystal symmetry. This parameter is not changed for the used hematite catalyst (used-Fe_2O_3 sample). The evolution of the hyperfine field and line width values agree with the decreasing particle sizes inferred from the XRD data. At the same time, the stable values of isomer shift confirm the chemical stability of the studied hematite catalyst.

3.1.3. SEM

The morphology of a catalyst surface plays an important role in catalytic reactions. The surface of the hematite Fe_2O_3 catalyst was analyzed by scanning electron microscopy. Fig. 4 shows the surface of hematite samples before and after sintering at 900 °C. It can be seen that the raw hematite particles are not uniform in shape and form large agglomerates. After sintering, a significant difference in

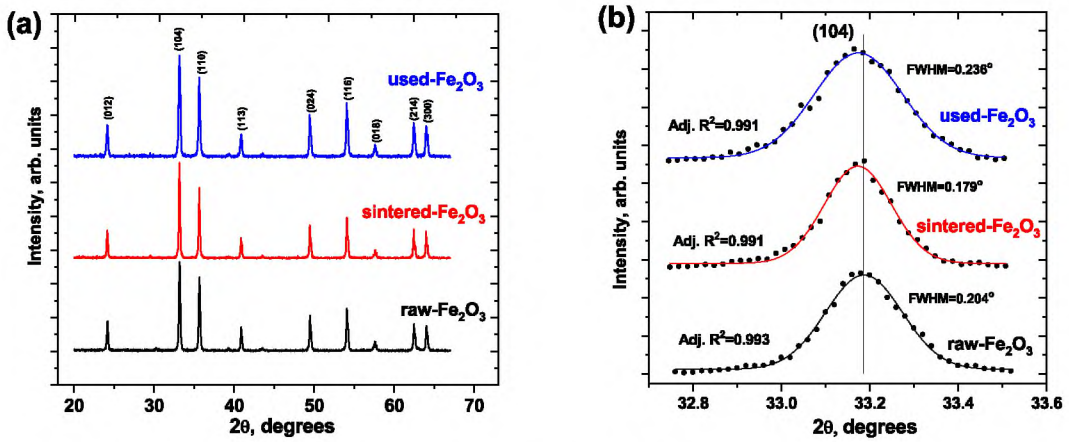

Fig. 2. (a) XRD patterns of the studied hematite samples; (b) the comparison of the (104) peaks for the hematite samples using Rietveld refinement.

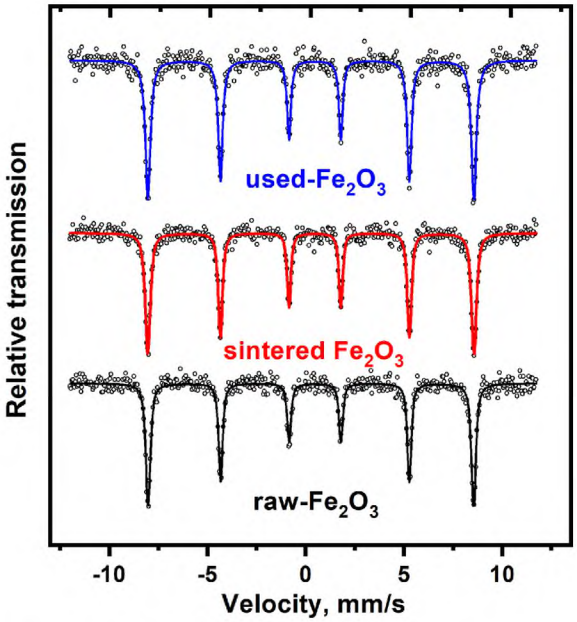

Fig. 3. Mössbauer spectra obtained at room temperature for the studied hematite samples.

morphology is observed. The fluffy surface of the raw-Fe_2O_3 sample became smooth in the sintered-Fe_2O_3 sample. This observation is in full agreement with the above explanation of the thermal dehydration of the hematite surface. The sintered-Fe_2O_3 particles assumed a spherical, slightly elongated shape. The morphology of the hematite catalyst after the catalytic reaction was also investigated. No visible changes in morphology were observed after the catalytic Fenton oxidation (Fig. 4). Both the shape and size of the hematite particles remain stable.

3.1.4. EDS

The method of energy-dispersive X-ray spectroscopy revealed the elemental composition of the hematite catalyst. Fig. 5 shows the EDS spectra of the raw-Fe_2O_3, sintered-Fe_2O_3, and used-Fe_2O_3 samples. In all three cases, the experimentally determined contents of O and Fe atoms are close to the ones theoretically predicted. No additional peaks of other elements were detected, which indicates the purity of the hematite phase.

3.2. Catalytic decomposition of hydrogen peroxide

3.2.1. Catalytic activity in batch mode

Comparative tests of the raw-Fe_2O_3 and sintered-Fe_2O_3 catalysts were carried out in batch mode. Fig. 6a shows the kinetic curves of H_2O_2 decomposition in the presence of the raw-Fe_2O_3 and sintered-Fe_2O_3 catalysts. The decomposition of H_2O_2 without a catalyst is very slow (Fig. 6a). Both the raw-Fe_2O_3 and sintered-Fe_2O_3 samples accelerate the decomposition of H_2O_2, with the former one having higher catalytic activity. The degree of decomposition of H_2O_2 after 240 min with the raw-Fe_2O_3 catalyst is 16.8 % while that with the sintered-Fe_2O_3 catalyst is 3.8 % (Fig. 6a). The kinetic lines in Fig. 6a are well-fitted by the first order kinetic model (Fig. 6b). The corresponding values of reaction rate constants are presented in Fig. 6b.

Fig. 6c shows that the oxidation–reduction potential (ORP) of H_2O_2 solutions decreases gradually over the reaction time. This trend can be explained by the decomposition of H_2O_2 and the corresponding decrease in the formation of reactive oxygen species (ROS). Iron oxides Fe_2O_3 and Fe_3O_4 are well known as effective catalysts for the decomposition of hydrogen peroxide [58]. With the participation of the catalyst surface, hydrogen peroxide H_2O_2 decomposes, generating free radicals [59]. The ORP data (Fig. 6c) confirm that the raw-Fe_2O_3 is a more active catalyst than the sintered-Fe_2O_3. However, the advantage of sintered hematite is its stable granular form, required for use in a flow-through reactor.

3.2.2. Catalytic activity in the flow mode

The fixed bed reactor experiments were carried out using the granulated sintered-Fe_2O_3 catalyst. The studied parameters included the contact time and concentrations of inlet solutions. The contact time resulted from the reactor geometry (Table 1). The different void volumes of reactors resulted in different residence times while the flow rate was constant. Fig. 7a, 7b, and 7c show UV spectra of the solutions passed through the flow reactors A, B, and C. Fig. 7d, 7e, and 7f show the calculated values of the degree of H_2O_2 decomposition. The data clearly show that the efficiency of H_2O_2 decomposition increases with the increasing contact time. Reactor A provides a degree of H_2O_2 decomposition as low as 18.5 % (Fig. 7d). The reactors B and C provide quite higher degrees of H_2O_2 decomposition equal to 80.8 % (Fig. 7e) and 93 % (Fig. 7f), respectively. These differences result from much longer times of contact with the catalyst surface (Table 1). Both reactors B and C require some time (approximately 30 min) to attain a stable degree of H_2O_2 decomposition (Fig. 7e and 7f). Probably, the catalyst surface requires some time to be fully hydroxylated. Fig. 7d, 7e, and 7f show also the effect of H_2O_2 concentration on the decomposition efficiency. As the concentration of H_2O_2 increases, the degree of H_2O_2 decomposition naturally decreases.

The stability of the sintered-Fe_2O_3 catalyst was tested in reactor C fed with a 2 mM solution of hydrogen peroxide. During 270 h, the efficiency of H_2O_2 decomposition decreased from 82.5 % to 75.8 % (Fig. 8).

3.3. Oxidative degradation of oxytetracycline

OTC is widely used tetracycline antibiotic, which found its broad application in aquaculture [49]. Recently oxytetracycline was found in the rivers and soils [60]. The presence of oxytetracycline in the environment has negative consequences, due to its ability to directly affect microorganisms and promote antibiotic resistance. Therefore, the removal of OTC from environment is of great practical significance. Reactor C was used to study the oxidative degradation of oxytetracycline (OTC). Again, the primary reaction is the decomposition of H_2O_2 catalyzed by the Fe_2O_3 surface. The formed hydroxyl radicals $HO^{\bullet}$ are powerful oxidants and react rapidly with OTC. It is worth noting that hydrogen peroxide without catalyst does not cause any significant degradation of OTC (Fig. 9a). In addition, the unchanged spectra of OTC in Fig. 9b-f indicate that OTC without H_2O_2 was not degraded after contact with the hematite catalyst surface. On the other hand, spectra of the reaction mixture of OTC with H_2O_2 were substantially changed (Fig. 9b-f). The observed decay in the UV bands characteristic of the OTC (Fig. 9) indicates that the molecular skeleton of OTC is destroyed. Obviously, the hematite surface catalyzes cleavage of H_2O_2 according to the Fenton reaction. The formed hydroxyl radicals react with OTC resulting in hydroxylation, oxidation, decar-

Table 3
Hyperfine interaction parameters obtained from the Mössbauer spectra fitting (I_S – isomeric shift; Q_S – quadrupole splitting; H – hyperfine field; G – line width).

sample	I_s, mm/s	Q_s, mm/s	H, kOe	G, mm/s
raw-Fe_2O_3	0.3675	−0.212	514.3	0.280
sintered-Fe_2O_3	0.3662	−0.206	515.3	0.312
used-Fe_2O_3	0.3662	−0.206	515.0	0.302

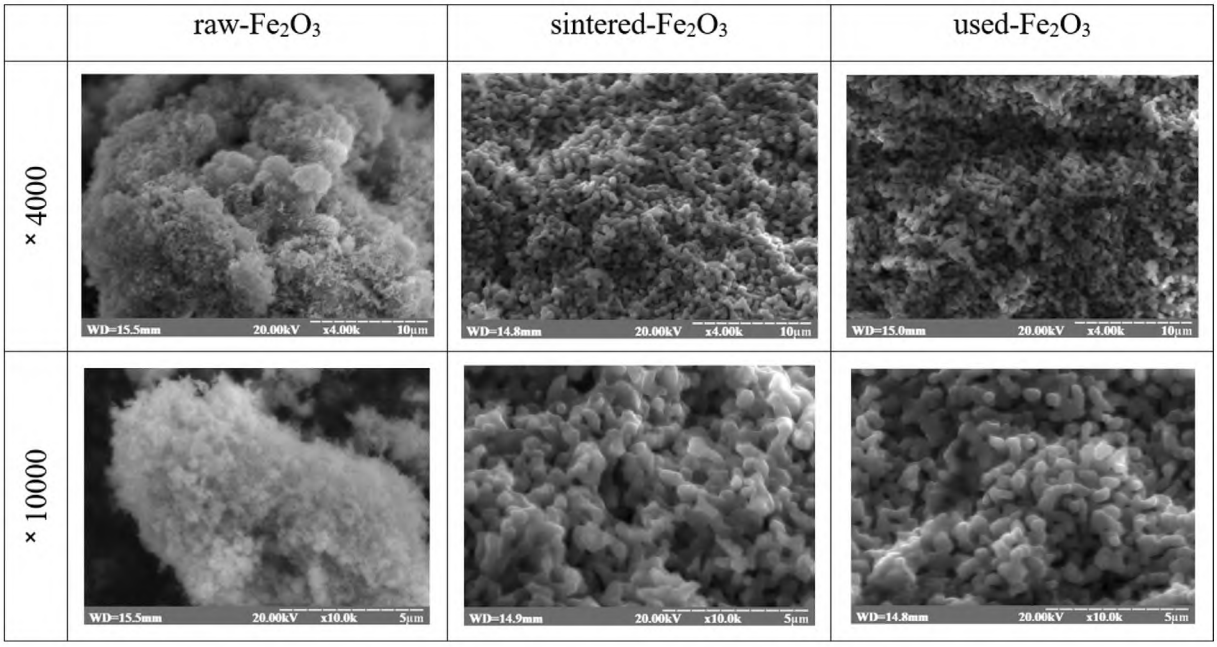

Fig. 4. SEM micrographs of the studied hematite catalyst samples at the magnifications × 4000 and × 10000.

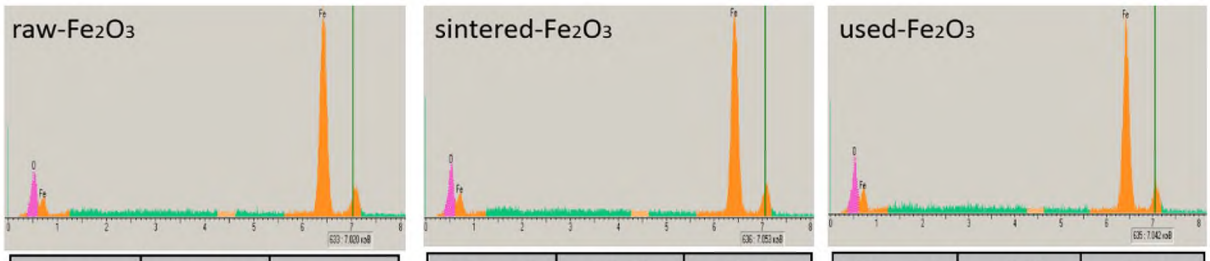

Element	wt. %	at. %
O	28.7	59.8
Fe	71.3	40.2

Element	wt. %	at. %
O	28.1	59.2
Fe	71.9	40.8

Element	wt. %	at. %
O	29.8	60.7
Fe	70.2	39.3

Fig. 5. Energy dispersive spectra and elemental composition of the studied Fe_2O_3 catalyst samples.

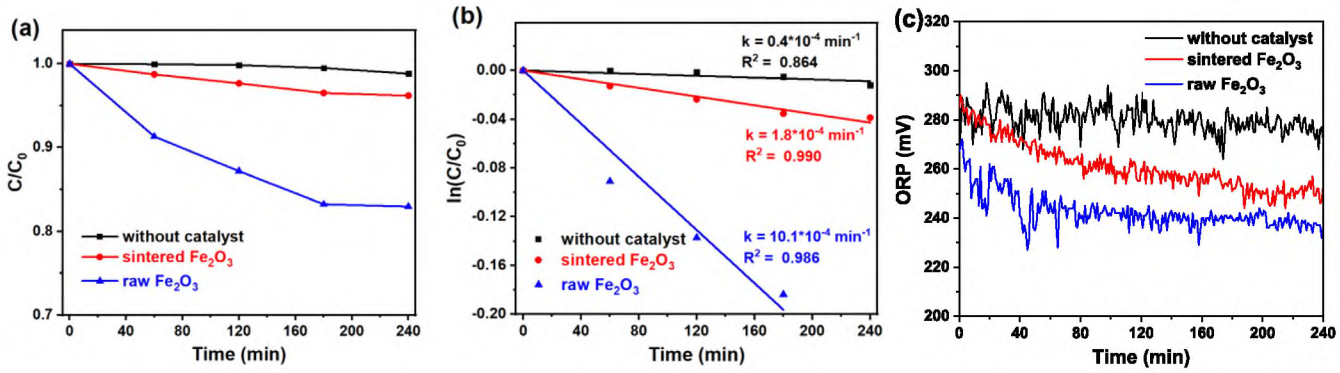

Fig. 6. H_2O_2 decomposition in the presence of the raw-Fe_2O_3 and sintered-Fe_2O_3 catalysts: (a) changes in H_2O_2 concentration *versus* reaction time; (b) transformed kinetic lines according to the first-order kinetic model; (c) changes of oxidation–reduction potential. The experimental conditions: initial concentration of H_2O_2 was 100 mM; the volume of H_2O_2 solution was 80 mL; catalyst dose was 160 mg.

bonylation and demethylation [50,61]. The most probable sites for hydroxylation (adding a hydroxyl group) are the phenyl ring and double bonds in the cyclohexene rings [61]. The oxidation takes place mainly by the abstraction of hydrogen atom from the secondary alcohol groups resulting in the ketone group. Decarbonylation results in formation of cyclopentene ring and two-step

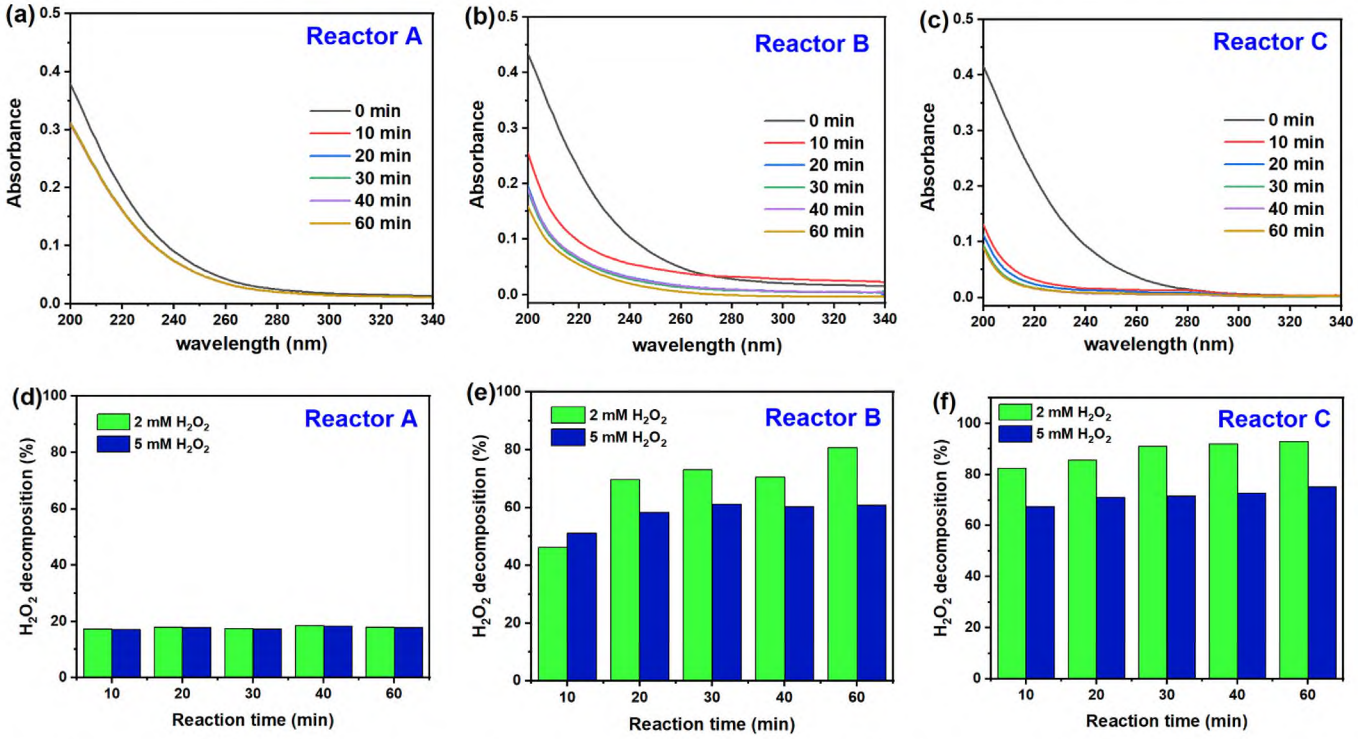

Fig. 7. (a,b,c) UV-spectra of the effluent solutions at inflow H_2O_2 concentration of 2 mM; (d,e,f) Impact of H_2O_2 concentration on the efficiency of H_2O_2 decomposition in the flow reactors.

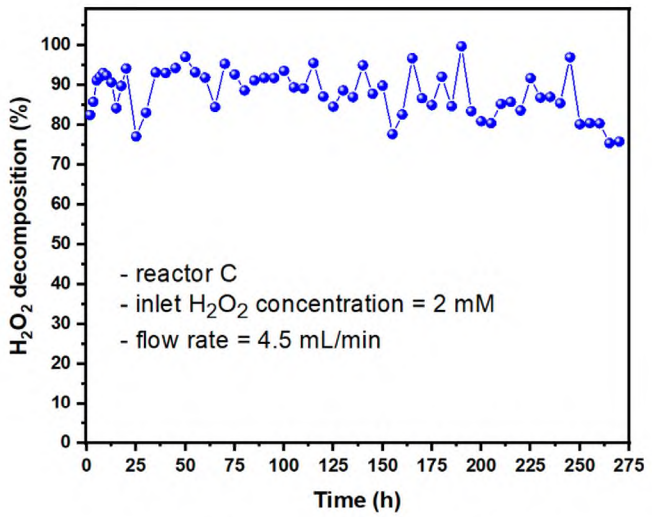

Fig. 8. Stability test of sintered-Fe_2O_3 catalyst.

demethylation of dimethylamine group results in primary amine group [50,61]. Fig. 10 shows that the degradation extent remains quite stable over time. This fact confirms the stable operating mode of the studied hematite catalyst.

The decomposition of OTC was investigated depending on the concentrations of the reactants at the reactor inlet. These relationships were quantified using the response surface methodology (RSM). RSM modeling provides mathematical equations that describe relationships between the parameters of interest (so-called response variables) and the experimental parameters (explanatory variables). In the present study, the response variable is the degree of oxytetracycline removal while the explanatory variables are initial H_2O_2 and OTC concentrations at the reactor inlet. The whole design consisted of 15 experiments (Table 2). Four mathematical models were tested to describe the extent of oxytetracycline degradation. The comparison results are summarized in the Supporting Information. The two-factor interaction model (2FI) was found to adequately describe the extent of oxytetracycline degradation:

$$OTC_{degradated}, \% = 62.89 + 3.56 \cdot C_{H_2O_2} - 8.96 \cdot C_{OTC} + 1.26 \cdot C_{H_2O_2} \cdot C_{OTC} \quad (6)$$

The statistical characteristics of the two-factor interaction model (6) are presented in the Supporting Information. Fig. 11a shows the corresponding response surface diagram. The predicted oxytetracycline removal efficiency fits well with the experimental values (Fig. 11b).

Fig. 11a depicts the effects of the concentrations of both reactants at the reactor inlet on the degradation efficiency. As the concentration of hydrogen peroxide increases, the degree of oxytetracycline removal naturally increases (Fig. 11a). The obvious cause is the increase in the amount of generated hydroxyl radicals. In contrast, an increase in oxytetracycline concentration has the opposite effect. The higher the concentration of oxytetracycline, the lower the percentage of oxytetracycline degradation (Fig. 11a). Both of these effects are quantified by the coefficients at the concentrations of H_2O_2 and OTC in Eq. (6). The third coefficient indicates a moderate positive synergy between H_2O_2 and OTC. The higher the concentrations of H_2O_2 and oxytetracycline, the higher the degree of OTC degradation. The spectra in Fig. 9 suggest that significant amounts of H_2O_2 remain in the outgoing solutions. This fact suggests that the degree of oxytetracycline degradation may be further increased when using larger catalyst mass or longer residence time.

3.4. Inactivation of bacteria E. Coli using the catalytic decomposition of H_2O_2

Reactive oxygen species (ROS) are well known to destroy bacterial cell walls [62–64]. This approach can be used for water disinfection [65,66]. Hematite catalyst can decompose hydrogen

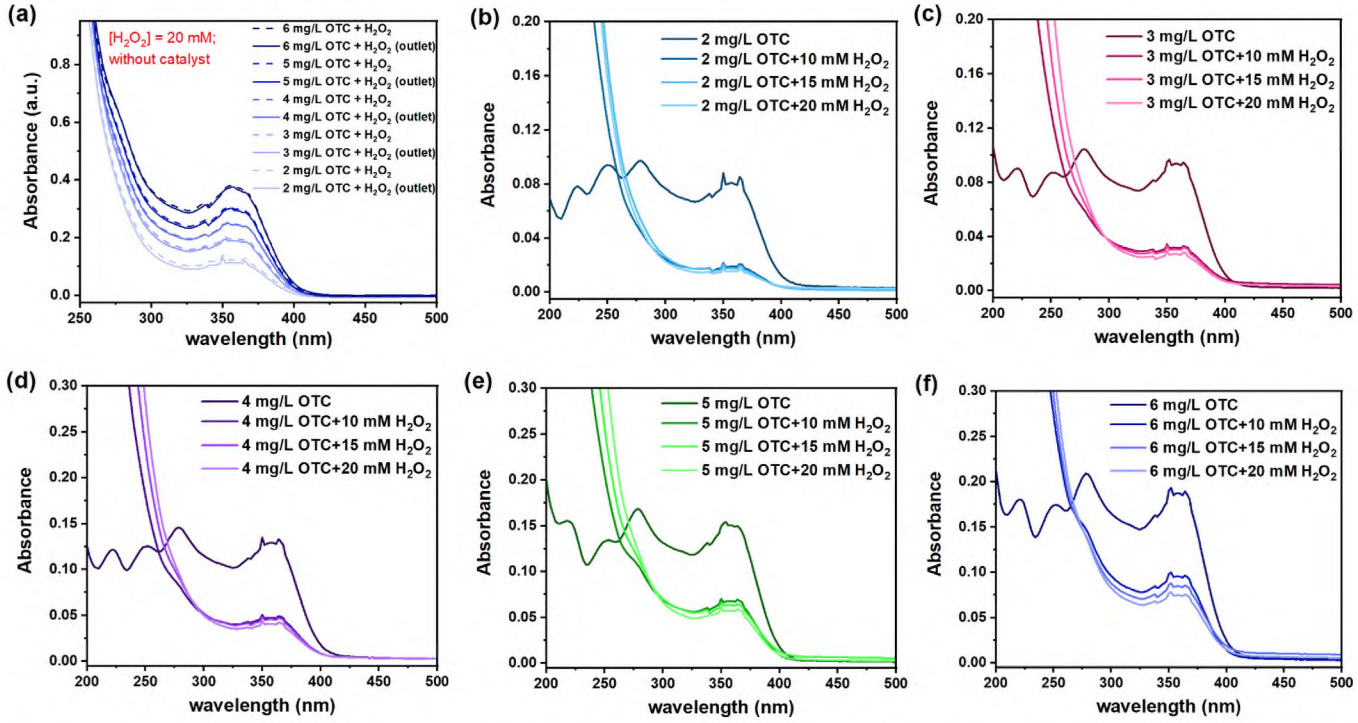

Fig. 9. (a) UV–vis spectra of the OTC and H_2O_2 mixtures without the hematite catalyst ([H_2O_2] = 20 mM); (b)-(f) UV–vis spectra of the reaction mixtures at the outlet of the reactor C together with the OTC spectrum. The inlet concentrations of OTC and H_2O_2 are indicated. Flow rate = 4.5 mL/min; temperature = 20 °C.

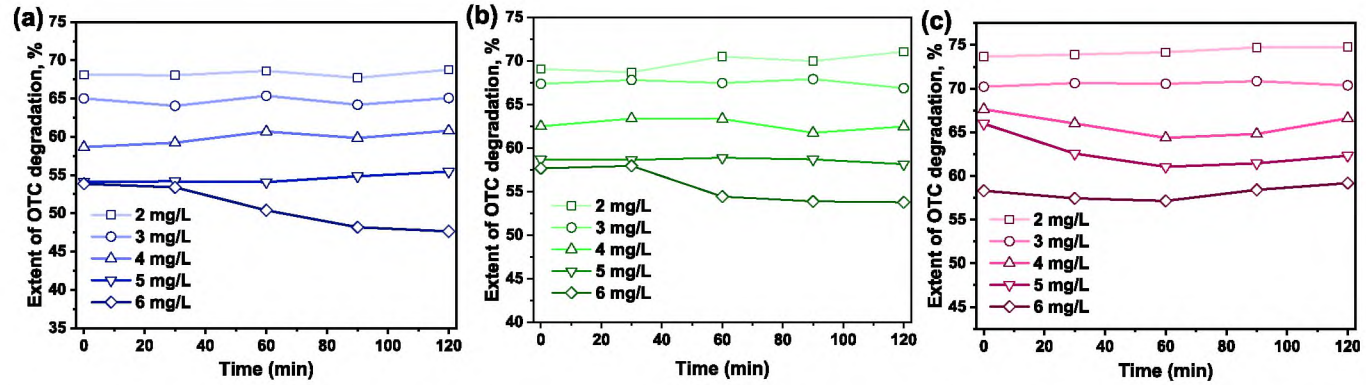

Fig. 10. The extent of OTC degradation *versus* time at different concentrations of H_2O_2 and OTC at the reactor C inlet: (a) 10 mM H_2O_2; (b) 15 mM H_2O_2; (c) 20 mM H_2O_2. Flow rate = 4.5 mL/min; temperature = 20 °C.

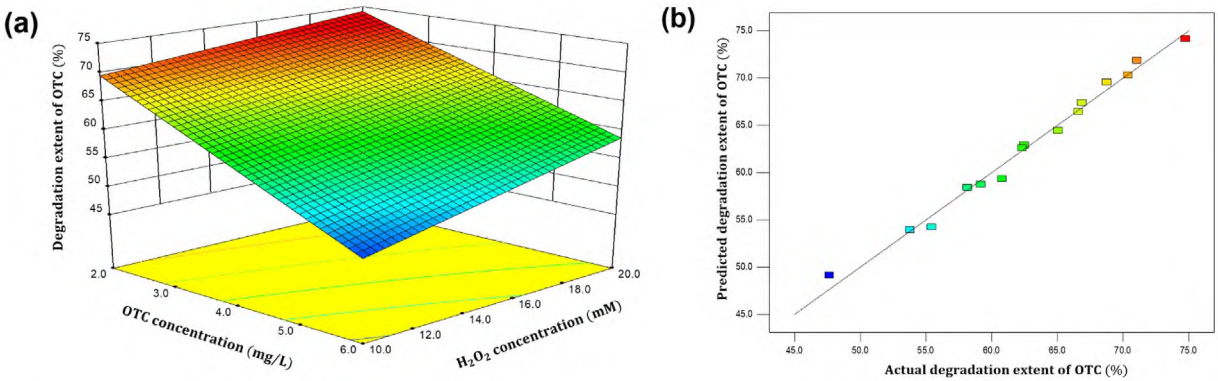

Fig. 11. (a) Response surface plot showing the degree of oxytetracycline removal depending on the concentrations of hydrogen peroxide and oxytetracycline at the reactor C inlet. (b) The predicted degree of oxytetracycline removal *versus* the experimental values.

peroxide H_2O_2 with concentrations up to 6 mol/L, causing the formation of radicals. The formed aggressive hydroxyl and hydroperoxyl radicals are good disinfectants [13]. In the present study, the heterogeneous hematite catalyst was tested for water disinfection using rather low concentrations of hydrogen peroxide. The aim was to maintain low outlet concentrations of H_2O_2 to minimize the possible danger for humans. Fig. 12 shows examples of the quantification of bacteria by colony counting.

Fig. 13a and 13b show the quantitative results of bacterial inactivation. The model suspensions contained live *E. coli* cells of 10^3, 10^4, and 10^5 CFU/L at the reactor inlet. The concentration of hydrogen peroxide from 10 to 200 mM was used. In the absence of a catalyst, the bacteria were not inactivated completely by hydrogen peroxide alone, as confirmed by control experiments. As the H_2O_2 concentration increases, the bacteria count at the outlet gradually decreases (Fig. 13a). The larger the inlet bacterial loading, the larger H_2O_2 concentration is required to attain an acceptable bacterial count in the purified water (approximately 10^1-10°CFU/L). It is quite obvious that the inactivation of a higher amount of bacteria requires a larger amount of reactive oxygen species to be generated [67]. For the complete inactivation of bacteria at 10^3 CFU/L, the inlet H_2O_2 concentration should be 150–200 mM. At larger inlet bacterial loadings, the bacteria counts were decreased by log values of about 2.4 (Fig. 13a). Fig. 13b shows the percentage of bacterial inactivation. With a low initial bacterial count of 10^3 CFU/L, 99 % inactivation efficiency is achieved with 25 mM H_2O_2. With a high bacterial count of 10^5 CFU/L, 99 % inactivation requires 100 mM hydrogen peroxide. The presented data show that the used flow reactor C with Fe_2O_3 catalyst provides an effective way for water disinfection.

Inactivation of bacteria by ROS in flow mode requires the maximization of the contact area between the catalyst and the bacteria in solution [68,69]. This approach was used for the inactivation of bacteria and SARS-CoV-2 viruses by the hematite-catalyzed

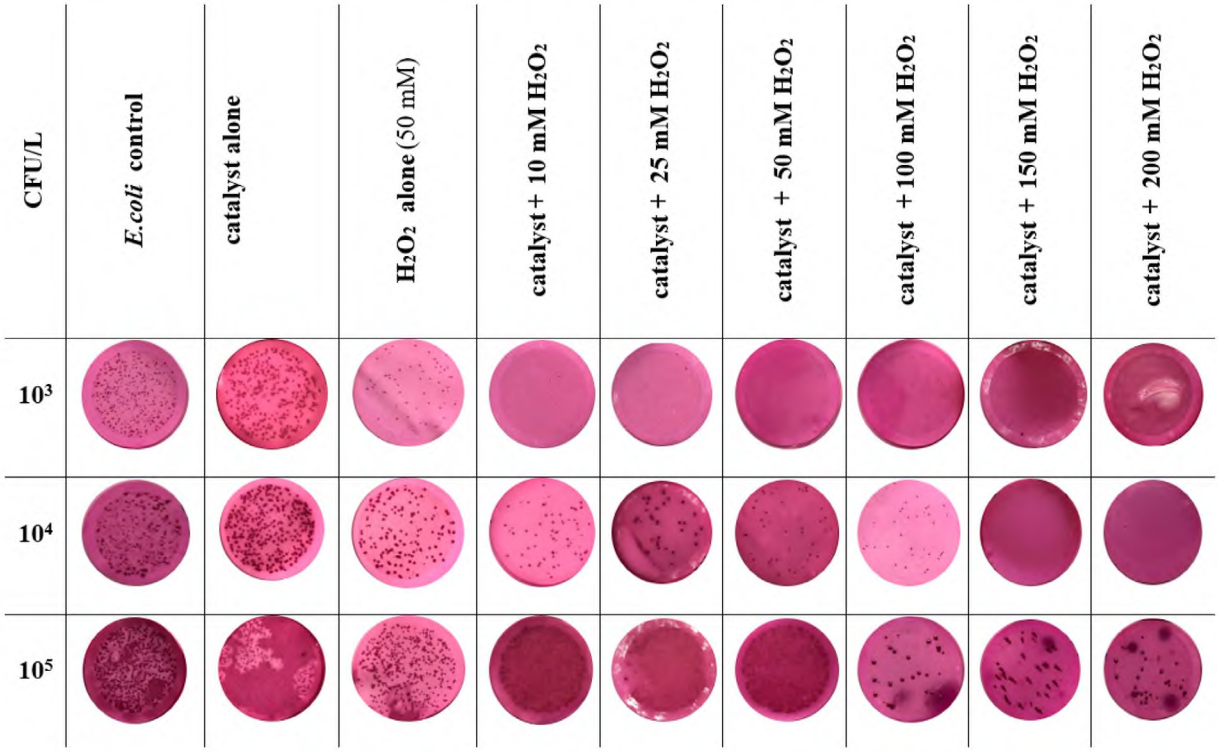

Fig. 12. Images of membrane filters with cultured bacterial colonies.

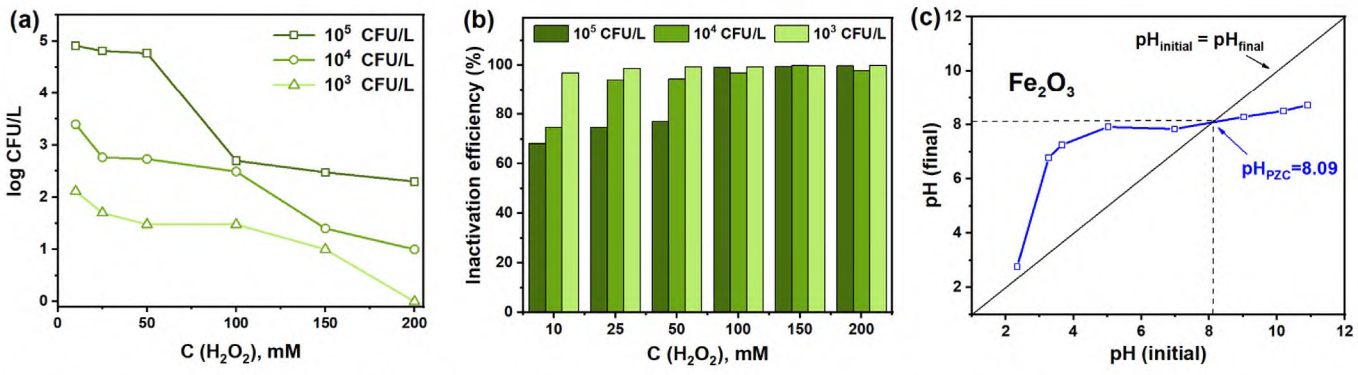

Fig. 13. The bacteria inactivation with the use of reactor C: (a) the bacterial count at the reactor C outlet depending on the bacterial count and H_2O_2 concentration at the inlet (flow rate = 4.5 mL/min; temperature = 20 °C); (b) the disinfection efficiency expressed in %; (c) the determination of the point of zero charge (pH_{PZC}) of the sintered hematite granules.

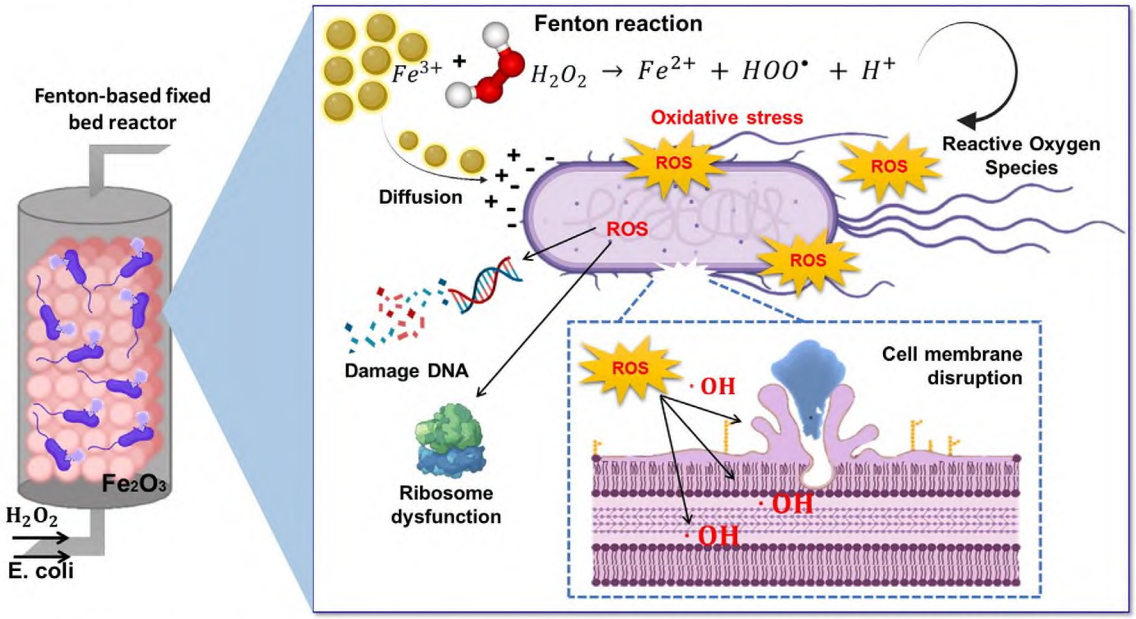

Fig. 14. Mechanism of *E. coli* inactivation by ROS generated by the decomposition of hydrogen peroxide on the hematite catalyst in a fixed-bed reactor.

decomposition of H_2O_2 [70]. Apart from oxidizing properties of hydroxyl radicals, the direct contact action of the hematite surface also provides some bacterial inactivation [68]. Usually, bacteria cell membranes carry a charge that causes an electrostatic attraction to solid surfaces [71]. Cell walls of Gram-positive bacteria (e.g., *S. aureus*, *Streptococcus mutans*) have a positive surface charge due to teichoic acid (a phosphate-containing polymer) [72]. Gram-negative bacteria (e.g., *P. aeruginosa, E. coli*) have a negative surface charge due to the dissociated carboxyl and phosphate groups of cell wall lipopolysaccharides. If the solid surface and the bacterial membrane have opposite charges, electrostatic attraction keeps the bacteria on the surface. If the charges have the same sign, electrostatic repulsion will prevent bacterial retention. In the present case, the charge of *E. coli* shells is negative while the charge of the hematite catalyst surface depends on the solution pH. The point of zero charge of the tested hematite catalyst was determined experimentally (Fig. 13c). The point of zero charge was found to be 8.09. In other words, the catalyst surface is positively charged at a pH below 8.09. In neutral solutions, *E. coli* is electrostatically attracted to the hematite catalyst surface. This Coulombic attraction contributes to accelerating the inactivation of bacteria by reactive oxygen species formed on the hematite surface. Fig. 14 shows the general mechanism of *E. coli* inactivation *via* hydrogen peroxide decomposition in the fixed-bed reactor. ROS formed on the hematite catalyst surface destroys bacterial cell walls and provides the effective inactivation of *E. coli*.

4. Conclusions

This work describes a method of water disinfection by the decomposition of H_2O_2 in a fixed bed reactor using heterogeneous Fenton oxidation. Among advanced oxidation processes, Fenton oxidation has the advantage of being simple in use. Hydrogen peroxide is an inexpensive oxidizing agent that is convenient to store and handle. The proposed flow reactor was filled with Fe_2O_3 granules providing the necessary catalytic activity. The heterogeneous Fenton catalyst was prepared and tested to decompose H_2O_2, inactivate bacteria *E. coli*, and degrade oxytetracycline. In contrast to the homogeneous Fenton catalyst, the proposed fixed-bed reactor has the advantage that it maintains a stable catalytic performance over time. Catalyst stability was tested by XRD, Mössbauer spectroscopy, SEM, and EDS. The X-ray diffraction patterns confirmed that the peaks correspond to the rhombohedral structure of α-Fe_2O_3, which indicates the stability of the catalyst phase after the catalytic process. The average crystallite size of the hematite before and after annealing was 41 nm and 47 nm, respectively. After the hetero-Fenton catalytic reaction, the average crystallite size was reduced to 35 nm. SEM revealed no changes in morphology after the catalytic hetero-Fenton reaction. EDS data confirmed the presence of only O and Fe elements in the stoichiometric ratio. The fixed-bed catalytic reactor has been proved to be suitable for the oxidative degradation of oxytetracycline. The OTC degradation percentage has been reached up to 75 % using 20 mM H_2O_2 solution. The relationship of the OTC degradation with the initial concentrations of reactants was described using Response Surface Methodology. The bacteria inactivation was studied depending on the inlet concentration of hydrogen peroxide and the initial concentration of viable cells. It was found that the outlet bacterial count gradually decreases with the increase of the inlet H_2O_2 concentration from 10 to 200 mM. The larger the inlet bacterial loading, the larger the H_2O_2 concentration is required to attain an acceptable bacteria count at the reactor outlet (approx. 10^1-10°CFU/L). The complete inactivation of bacteria at 10^3 CFU/L needs the inlet H_2O_2 concentration of 200 mM. The general inference is that the decomposition of hydrogen peroxide on a hematite catalyst may be used for the degradation of organic pollutants and water disinfection.

CRediT authorship contribution statement

Tetiana Tatarchuk: Supervision, Visualization, Conceptualization, Investigation, Methodology, Project administration, Writing – original draft, Writing – review & editing. **Alexander Shyichuk:** Writing – original draft, Writing – review & editing. **Volodymyr Kotsyubynsky:** Investigation, Writing – original draft, Writing – review & editing. **Volodymyra Boiychuk:** Investigation.

Data availability

No data was used for the research described in the article.

Declaration of Competing Interest

The authors declare that they have no known competing financial interests or personal relationships that could have appeared to influence the work reported in this paper.

Acknowledgment

TT would like to acknowledge the support given by the National Science Centre (Poland) (project UMO-2022/01/3/ST5/00136).

References

[1] N. Verma, S. Vaidh, G.S. Vishwakarma, A. Pandya, Antimicrobial nanomaterials for water disinfection, Nanotoxicity. (2020) 365–383, https://doi.org/10.1016/b978-0-12-819943-5.00018-x.
[2] F.R. Rijsberman, Water scarcity: Fact or fiction?, Agric Water Manag. 80 (2006) 5–22, https://doi.org/10.1016/j.agwat.2005.07.001.
[3] J.W. St. Geme, K.A. Rempe, Classification of Bacteria, Fifth Edit, Elsevier Inc., 2018. https://doi.org/10.1016/B978-0-323-40181-4.00114-6.
[4] A. Mai-Prochnow, M. Clauson, J. Hong, A.B. Murphy, Gram positive and Gram negative bacteria differ in their sensitivity to cold plasma, Sci. Rep. 6 (2016) 1–11, https://doi.org/10.1038/srep38610.
[5] A. Basu, M. Behera, R. Maharana, M. Kumar, N.K. Dhal, A.J. Tamhankar, A. Mishra, C. Stålsby Lundborg, S.K. Tripathy, To unsnarl the mechanism of disinfection of Escherichia coli via visible light assisted heterogeneous photo-Fenton reaction in presence of biochar supported maghemite nanoparticles, J. Environ Chem. Eng. 9 (1) (2021) 104620.
[6] T. Tatarchuk, A. Shyichuk, I. Trawczyńska, I. Yaremiy, A.T. Pędziwiatr, P. Kurzydło, B.F. Bogacz, R. Gargula, Spinel cobalt(II) ferrite-chromites as catalysts for H2O2 decomposition: Synthesis, morphology, cation distribution and antistructure model of active centers formation, Ceram. Int. 46 (2020) 27517–27530, https://doi.org/10.1016/j.ceramint.2020.07.243.
[7] K. Czyzewska, A. Trusek-Holownia, M. Dabrowa, F. Sarmiento, J.M. Blamey, A catalytic membrane used for H2O2 decomposition, Catal. Today. (2019) 30–34, https://doi.org/10.1016/j.cattod.2017.11.025.
[8] T. Tatarchuk, N. Danyliuk, A. Shyichuk, V. Kotsyubynsky, I. Lapchuk, V. Mandzyuk, Green synthesis of cobalt ferrite using grape extract: the impact of cation distribution and inversion degree on the catalytic activity in the decomposition of hydrogen peroxide, Emergent Mater. 5 (1) (2022) 89–103.
[9] T. Tatarchuk, N. Danyliuk, V. Kotsyubynsky, A. Shumskaya, E. Kaniukov, A.A. Ghfar, M. Naushad, A. Shyichuk, Eco-friendly synthesis of cobalt-zinc ferrites using quince extract for adsorption and catalytic applications : An approach towards environmental remediation, Chemosphere. 294 (2022), https://doi.org/10.1016/j.chemosphere.2022.133565 133565.
[10] T. Tatarchuk, N. Danyliuk, I. Lapchuk, A. Shyichuk, V. Kotsyubynsky, Catalytic activity of magnetite and its magnetic heating properties, Mater. Today Proc. 62 (2022) 5805–5811.
[11] N. Danyliuk, S. Lischynska, T. Tatarchuk, V. Kotsyubynsky, V. Mandzyuk, Magnetite nanoparticles synthesized using grape fruit extract: synthesis, morphology, hyperthermia application and catalytic activity in hydrogen peroxide decomposition, Phys. Chem. Solid State. 23 (2022) 77–88, https://doi.org/10.15330/pcss.23.1.77-88.
[12] X. Huang, X. Hou, J. Zhao, L. Zhang, Hematite facet confined ferrous ions as high efficient Fenton catalysts to degrade organic contaminants by lowering H2O2 decomposition energetic span, Appl. Catal. B Environ. 181 (2016) 127–137, https://doi.org/10.1016/J.APCATB.2015.06.061.
[13] Y. Zhu, R. Zhu, Y. Xi, J. Zhu, G. Zhu, H. He, Strategies for enhancing the heterogeneous fenton catalytic reactivity: A review, Appl. Catal. B Environ. 255 (2019), https://doi.org/10.1016/j.apcatb.2019.05.041 117739.
[14] E.G. Garrido-Ramírez, B.K.G. Theng, M.L. Mora, Clays and oxide minerals as catalysts and nanocatalysts in Fenton-like reactions - A review, Appl. Clay Sci. 47 (2010) 182–192, https://doi.org/10.1016/j.clay.2009.11.044.
[15] P. Baldrian, V. Merhautová, J. Gabriel, F. Nerud, P. Stopka, M. Hrubý, M.J. Beneš, Decolorization of synthetic dyes by hydrogen peroxide with heterogeneous catalysis by mixed iron oxides, Appl. Catal. B Environ. 66 (2006) 258–264, https://doi.org/10.1016/j.apcatb.2006.04.001.
[16] P.V. Nidheesh, Heterogeneous Fenton catalysts for the abatement of organic pollutants from aqueous solution: A review, RSC Adv. 5 (2015) 40552–40577, https://doi.org/10.1039/c5ra02023a.
[17] A. Rufus, N. Sreeju, D. Philip, Size tunable biosynthesis and luminescence quenching of nanostructured hematite (α-Fe2O3) for catalytic degradation of organic pollutants, J. Phys. Chem. Solids. 124 (2019) 221–234, https://doi.org/10.1016/j.jpcs.2018.09.026.
[18] L. Lai, Y. He, H. Zhou, B. Huang, G. Yao, B. Lai, Critical review of natural iron-based minerals used as heterogeneous catalysts in peroxide activation processes: Characteristics, applications and mechanisms, J. Hazard. Mater. 416 (2021), https://doi.org/10.1016/j.jhazmat.2021.125809 125809.
[19] J. Liu, C. Peng, X. Shi, Preparation, characterization, and applications of Fe-based catalysts in advanced oxidation processes for organics removal: A review, Environ. Pollut. 293 (2022), https://doi.org/10.1016/j.envpol.2021.118565 118565.
[20] A. Nadar, A.M. Banerjee, M.R. Pai, S.S. Meena, R.V. Pai, R. Tewari, S.M. Yusuf, A. K. Tripathi, S.R. Bharadwaj, Nanostructured Fe2O3 dispersed on SiO2 as catalyst for high temperature sulfuric acid decomposition—Structural and morphological modifications on catalytic use and relevance of Fe2O3-SiO2 interactions, Appl. Catal. B Environ. 217 (2017) 154–168, https://doi.org/10.1016/j.apcatb.2017.05.045.
[21] A. Nadar, A.M. Banerjee, M.R. Pai, S.S. Meena, A.K. Patra, P.U. Sastry, R. Singh, M. K. Singh, A.K. Tripathi, Immobilization of crystalline Fe2O3 nanoparticles over SiO2 for creating an active and stable catalyst: A demand for high temperature sulfuric acid decomposition, Appl. Catal. B Environ. 283 (2021), https://doi.org/10.1016/j.apcatb.2020.119610 119610.
[22] X. liu, Progress in the Mechanism and Kinetics of Fenton Reaction, MOJ Ecol. Environ. Sci. 3 (2018) 10–14. https://doi.org/10.15406/mojes.2018.03.00060.
[23] N. Thomas, D.D. Dionysiou, S.C. Pillai, Heterogeneous Fenton catalysts: A review of recent advances, J. Hazard. Mater. 404 (2021), https://doi.org/10.1016/j.jhazmat.2020.124082 124082.
[24] T. Tsuneda, Fenton reaction mechanism generating no OH radicals in Nafion membrane decomposition, Sci. Rep. 10 (2020) 1–13, https://doi.org/10.1038/s41598-020-74646-0.
[25] G. Zhao, L. Liang, E. Wang, S. Lou, R. Qi, R. Tong, Fenton chemistry enables the catalytic oxidative rearrangement of indoles using hydrogen peroxide, Green Chem. 23 (2021) 2300–2307, https://doi.org/10.1039/d1gc00297j.
[26] M.L. Kremer, Mechanism of the Fenton reaction. Evidence for a new intermediate, Phys. Chem. Chem. Phys. 1 (1999) 3595–3605, https://doi.org/10.1039/a903915e.
[27] G. Centi, S. Perathoner, T. Torre, M.G. Verduna, Catalytic wet oxidation with H2O2 of carboxylic acids on homogeneous and heterogeneous Fenton-type catalysts, Catal. Today. 55 (2000) 61–69, https://doi.org/10.1016/S0920-5861(99)00226-6.
[28] A. Grunert, A. Frohnert, H.C. Selinka, R. Szewzyk, A new approach to testing the efficacy of drinking water disinfectants, Int. J. Hyg. Environ. Health. 221 (2018) 1124–1132, https://doi.org/10.1016/j.ijheh.2018.07.010.
[29] M.I. Pariente, R. Molina, J.A. Melero, J.Á. Botas, F. Martínez, Intensified-Fenton process for the treatment of phenol aqueous solutions, Water Sci. Technol. 71 (2015) 359–365, https://doi.org/10.2166/wst.2014.515.
[30] Y. Shao, H. Chen, Heterogeneous Fenton oxidation of phenol in fixed-bed reactor using Fe nanoparticles embedded within ordered mesoporous carbons, Chem. Eng. Res. Des. 132 (2018) 57–68, https://doi.org/10.1016/j.cherd.2017.12.039.
[31] J. Marugán, R. van Grieken, C. Pablos, M.L. Satuf, A.E. Cassano, O.M. Alfano, Photocatalytic inactivation of Escherichia coli aqueous suspensions in a fixed-bed reactor, Catal. Today. 252 (2015) 143–149, https://doi.org/10.1016/j.cattod.2014.10.031.
[32] S. Punathil, D. Ghime, T. Mohapatra, C. Thakur, P. Ghosh, Fixed Bed Reactor for Removal of Methylene Blue Dye Using Heterogeneous Fenton Catalyst, J. Hazardous, Toxic, Radioact. Waste. 24 (2020) 04020037, https://doi.org/10.1061/(asce)hz.2153-5515.0000534.
[33] M. Munoz, J. Nieto-Sandoval, E. Serrano, Z.M. de Pedro, J.A. Casas, CWPO intensification by induction heating using magnetite as catalyst, J. Environ. Chem. Eng. 8 (5) (2020) 104085.
[34] X. Xu, W. Chen, S. Zong, X. Ren, D. Liu, Magnetic clay as catalyst applied to organics degradation in a combined adsorption and Fenton-like process, Chem. Eng. J. 373 (2019) 140–149, https://doi.org/10.1016/j.cej.2019.05.030.
[35] A.T. Vu, T.N. Xuan, C.H. Lee, Preparation of mesoporous Fe2O3·SiO2 composite from rice husk as an efficient heterogeneous Fenton-like catalyst for degradation of organic dyes, J. Water Process Eng. 28 (2019) 169–180, https://doi.org/10.1016/j.jwpe.2019.01.019.
[36] P. Zolfaghari, M. Aghbolaghy, A. Karimi, A. Khataee, Continuous degradation of an organic pollutant using heterogeneous magnetic biocatalyst and CFD analysis of the process, Process Saf. Environ. Prot. 121 (2019) 338–348, https://doi.org/10.1016/j.psep.2018.11.004.
[37] P. Dash, S. Raut, M. Jena, B. Nayak, Harnessing the biomedical properties of ferromagnetic α-Fe2O3 NPs with a plausible formation mechanism, Ceram. Int. 46 (2020) 26190–26204, https://doi.org/10.1016/j.ceramint.2020.07.117.
[38] P.S. Sundara Selvam, S. Govindan, B. Perumal, V. Kandan, Screening of In Vitro Antibacterial Property of Hematite (α-Fe2O3) Nanoparticles: A Green Approach, Iran. J. Sci. Technol. Trans. A Sci. 45 (2021) 177–187, https://doi.org/10.1007/s40995-020-00995-0.
[39] S. Vihodceva, A. Šutka, M. Sihtmäe, M. Rosenberg, M. Otsus, I. Kurvet, K. Smits, L. Bikse, A. Kahru, K. Kasemets, Antibacterial activity of positively and negatively charged hematite (α-fe2 o3) nanoparticles to escherichia coli, staphylococcus aureus and vibrio fischeri, Nanomaterials. 11 (2021) 1–26, https://doi.org/10.3390/nano11030652.
[40] S. Natarajan, K. Harini, G.P. Gajula, B. Sarmento, M.T. Neves-Petersen, V. Thiagarajan, Multifunctional magnetic iron oxide nanoparticles: diverse synthetic approaches, surface modifications, cytotoxicity towards biomedical and industrial applications, BMC Mater. 1 (2019) 1–22, https://doi.org/10.1186/s42833-019-0002-6.
[41] M.A. Silva, C.V. Rocha, J. Gallo, H.P. Felgueiras, M.T.P. de Amorim, Porous composites based on cellulose acetate and alfa-hematite with optical and antimicrobial properties, Carbohydr. Polym. 241 (2020), https://doi.org/10.1016/j.carbpol.2020.116362 116362.
[42] A. Rufus, N. Sreeju, V. Vilas, D. Philip, Biosynthesis of hematite (α-Fe2O3) nanostructures: Size effects on applications in thermal conductivity, catalysis, and antibacterial activity, J. Mol. Liq. 242 (2017) 537–549, https://doi.org/10.1016/j.molliq.2017.07.057.

[43] K. Tharani, A. Jegatha Christy, S. Sagadevan, L.C. Nehru, Photocatalytic and antibacterial performance of iron oxide nanoparticles formed by the combustion method, Chem. Phys. Lett. 771 (2021), https://doi.org/10.1016/j.cplett.2021.138524 138524.
[44] A. Azam, A.S. Ahmed, M. Oves, M.S. Khan, S.S. Habib, A. Memic, Antimicrobial activity of metal oxide nanoparticles against Gram-positive and Gram-negative bacteria: A comparative study, Int. J. Nanomedicine. 7 (2012) 6003–6009, https://doi.org/10.2147/IJN.S35347.
[45] M. Bhushan, Y. Kumar, L. Periyasamy, A.K. Viswanath, Antibacterial applications of α-Fe2O3/Co3O4 nanocomposites and study of their structural, optical, magnetic and cytotoxic characteristics, Appl. Nanosci. 8 (2018) 137–153, https://doi.org/10.1007/s13204-018-0656-5.
[46] J.F. Leal, E.B.H. Santos, V.I. Esteves, Oxytetracycline in intensive aquaculture: water quality during and after its administration, environmental fate, toxicity and bacterial resistance, Rev. Aquac. 11 (2019) 1176–1194, https://doi.org/10.1111/raq.12286.
[47] M. Ghanbari, V. Klose, F. Crispie, P.D. Cotter, The dynamics of the antibiotic resistome in the feces of freshly weaned pigs following therapeutic administration of oxytetracycline, Sci. Rep. 9 (2019) 4062, https://doi.org/10.1038/s41598-019-40496-8.
[48] X. Wang, Y. Lin, Y. Zheng, F. Meng, Antibiotics in mariculture systems: A review of occurrence, environmental behavior, and ecological effects, Environ. Pollut. 293 (2022), https://doi.org/10.1016/j.envpol.2021.118541 118541.
[49] Z. Li, W. Qi, Y. Feng, Y. Liu, S. Ebrahim, J. Long, Degradation mechanisms of oxytetracycline in the environment, J. Integr. Agric. 18 (2019) 1953–1960, https://doi.org/10.1016/S2095-3119(18)62121-5.
[50] Y. Liu, X. He, Y. Fu, D.D. Dionysiou, Degradation kinetics and mechanism of oxytetracycline by hydroxyl radical-based advanced oxidation processes, Chem. Eng. J. 284 (2016) 1317–1327, https://doi.org/10.1016/j.cej.2015.09.034.
[51] P. Raizada, J. Kumari, P. Shandilya, R. Dhiman, V. Pratap Singh, P. Singh, Magnetically retrievable Bi2WO6/Fe3O4 immobilized on graphene sand composite for investigation of photocatalytic mineralization of oxytetracycline and ampicillin, Process Saf. Environ. Prot. 106 (2017) 104–116, https://doi.org/10.1016/j.psep.2016.12.012.
[52] M. Zouanti, M. Bezzina, R. Dhib, Experimental study of degradation and biodegradability of oxytetracycline antibiotic in aqueous solution using Fenton process, Environ. Eng. Res. 25 (2020) 316–323, https://doi.org/10.4491/eer.2018.343.
[53] K. Ulucan-Altuntas, S. Yazici Guvenc, E. Can-Güven, F. Ilhan, G. Varank, Degradation of oxytetracycline in aqueous solution by heat-activated peroxydisulfate and peroxymonosulfate oxidation, Environ. Sci. Pollut. Res. 29 (2022) 9110–9123, https://doi.org/10.1007/s11356-021-16157-7.
[54] C. Du, Y. Zhang, Z. Zhang, D. Song, J. Cao, H. Yu, G. Yu, L. Zhou, Y. Su, Y. Lv, H. Zhu, F. Deng, Highly efficient removal of oxytetracycline using activated magnetic MIL-101(Fe)/γ-Fe2O3 heterojunction catalyst, J. Environ. Manage. 317 (2022), https://doi.org/10.1016/j.jenvman.2022.115327 115327.
[55] Y.-J. Lee, C.-G. Lee, S.-J. Park, E.H. Jho, Degradation of Oxytetracycline by Persulfate Activation Using a Magnetic Separable Iron Oxide Catalyst Derived from Hand-Warmer Waste, Appl. Sci. 11 (21) (2021) 10447.
[56] H. Xue, M. Li, B. Liu, Q. Meng, Photochemical degradation kinetics and mechanisms of norfloxacin and oxytetracycline, Environ. Sci. Pollut. Res. 28 (2021) 8258–8265, https://doi.org/10.1007/s11356-020-11181-5.
[57] C. Zhang, G. Ren, W. Wang, X. Yu, F. Yu, Q. Zhang, M. Zhou, A new type of continuous-flow heterogeneous electro-Fenton reactor for Tartrazine degradation, Sep. Purif. Technol. 208 (2019) 76–82, https://doi.org/10.1016/j.seppur.2018.05.016.
[58] K. Barbusiński, Fenton reaction - Controversy concerning the chemistry, Ecol. Chem. Eng. S. 16 (2009) 347–358.
[59] M. Xu, C. Wu, Y. Zhou, Advancements in the Fenton Process for Wastewater Treatment, Adv. Oxid. Process. - Appl. Trends, Prospect. (2020), https://doi.org/10.5772/intechopen.90256.
[60] X. Liu, Y. Pei, M. Cao, H. Yang, Y. Li, Highly dispersed copper single-atom catalysts activated peroxymonosulfate for oxytetracycline removal from water: Mechanism and degradation pathway, Chem. Eng. J. 450 (2022), https://doi.org/10.1016/j.cej.2022.138194 138194.
[61] C.-H. Han, H.-D. Park, S.-B. Kim, V. Yargeau, J.-W. Choi, S.-H. Lee, J.-A. Park, Oxidation of tetracycline and oxytetracycline for the photo-Fenton process: Their transformation products and toxicity assessment, Water Res. 172 (2020), https://doi.org/10.1016/j.watres.2020.115514 115514.
[62] F. Vatansever, W.C.M.A. de Melo, P. Avci, D. Vecchio, M. Sadasivam, A. Gupta, R. Chandran, M. Karimi, N.A. Parizotto, R. Yin, G.P. Tegos, M.R. Hamblin, Antimicrobial strategies centered around reactive oxygen species - bactericidal antibiotics, photodynamic therapy, and beyond, FEMS Microbiol. Rev. 37 (2013) 955–989, https://doi.org/10.1111/1574-6976.12026.
[63] Y. Hong, J. Zeng, X. Wang, K. Drlica, X. Zhao, Post-stress bacterial cell death mediated by reactive oxygen species, Proc. Natl. Acad. Sci. U. S. A. 116 (2019) 10064–10071, https://doi.org/10.1073/pnas.1901730116.
[64] X. Zhao, K. Drlica, Reactive oxygen species and the bacterial response to lethal stress, Curr. Opin. Microbiol. 21 (2014) 1–6, https://doi.org/10.1016/j.mib.2014.06.008.
[65] A. Kawano, R. Yamasaki, T. Sakakura, Y. Takatsuji, T. Haruyama, Y. Yoshioka, W. Ariyoshi, Reactive Oxygen Species Penetrate Persister Cell Membranes of Escherichia coli for Effective Cell Killing, Front. Cell. Infect. Microbiol. 10 (2020) 1–13, https://doi.org/10.3389/fcimb.2020.00496.
[66] Y. Zhao, Z.-X. Low, Y. Pan, Z. Zhong, G. Gao, Universal water disinfection by piezoelectret aluminium oxide-based electroporation and generation of reactive oxygen species, Nano Energy. 92 (2022), https://doi.org/10.1016/j.nanoen.2021.106749 106749.
[67] C. Pablos, R. Van Grieken, J. Marugán, B. Moreno, Photocatalytic inactivation of bacteria in a fixed-bed reactor: Mechanistic insights by epifluorescence microscopy, Catal. Today. 161 (2011) 133–139, https://doi.org/10.1016/j.cattod.2010.10.051.
[68] R.A. Ismail, G.M. Sulaiman, S.A. Abdulrahman, T.R. Marzoog, Antibacterial activity of magnetic iron oxide nanoparticles synthesized by laser ablation in liquid, Mater. Sci. Eng. C. 53 (2015) 286–297, https://doi.org/10.1016/j.msec.2015.04.047.
[69] J.S. Kim, E. Kuk, K.N. Yu, J.H. Kim, S.J. Park, H.J. Lee, S.H. Kim, Y.K. Park, Y.H. Park, C.Y. Hwang, Y.K. Kim, Y.S. Lee, D.H. Jeong, M.H. Cho, Antimicrobial effects of silver nanoparticles, Nanomedicine Nanotechnology, Biol. Med. 3 (2007) 95–101, https://doi.org/10.1016/j.nano.2006.12.001.
[70] A. Shishkin, G. Goel, J. Baronins, J. Ozolins, C. Hoskins, S. Goel, Using circular economy principles to recycle materials in guiding the design of a wet scrubber-reactor for indoor air disinfection from coronavirus and other pathogens, Environ. Technol. Innov. 22 (2021), https://doi.org/10.1016/j.eti.2021.101429 101429.
[71] L. Yeh, C.-H. Yen, Y.-L. Kao, H.-L. Lien, S. Chang, Inactivation of Escherichia coli by dual-functional zerovalent Fe/Al composites in water, Chemosphere. 299 (2022), https://doi.org/10.1016/j.chemosphere.2022.134371 134371.
[72] M. Wang, Z. Li, Y. Zhang, Y. Li, N.a. Li, D. Huang, B. Xu, Interaction with teichoic acids contributes to highly effective antibacterial activity of graphene oxide on Gram-positive bacteria, J. Hazard. Mater. 412 (2021) 125333.